

CrystEngComm

Accepted Manuscript



This is an *Accepted Manuscript*, which has been through the Royal Society of Chemistry peer review process and has been accepted for publication.

Accepted Manuscripts are published online shortly after acceptance, before technical editing, formatting and proof reading. Using this free service, authors can make their results available to the community, in citable form, before we publish the edited article. We will replace this *Accepted Manuscript* with the edited and formatted *Advance Article* as soon as it is available.

You can find more information about *Accepted Manuscripts* in the [Information for Authors](#).

Please note that technical editing may introduce minor changes to the text and/or graphics, which may alter content. The journal's standard [Terms & Conditions](#) and the [Ethical guidelines](#) still apply. In no event shall the Royal Society of Chemistry be held responsible for any errors or omissions in this *Accepted Manuscript* or any consequences arising from the use of any information it contains.

Crosslinking of the Pd(acacCN)₂ building unit with Ag(I) salts: dynamic 1D polymers and an extended 3D network[†]

Qianqian Guo,^a Carina Merckens,^a Runze Si,^b and Ulli Englert^{*a}

Received Xth XXXXXXXXXX 20XX, Accepted Xth XXXXXXXXXX 20XX

First published on the web Xth XXXXXXXXXX 200X

DOI: 10.1039/b000000x

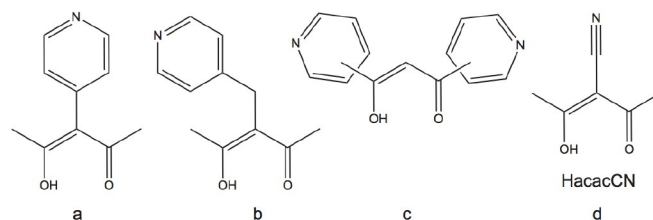
After deprotonation, the acetylacetonate moiety of the ditopic ligand 3-cyanoacetylacetonate (HacacCN) acts as a chelating ligand towards Pd(II). The resulting square-planar complex Pd(acacCN)₂ represents a suitable building unit for extended structures via coordination of Ag(I) cations to the peripheral nitrile groups. These target compounds have been structurally characterized: With silver salts of the anions BF₄⁻, ClO₄⁻, PF₆⁻ and CF₃SO₃⁻, chain polymers with an alternating sequence of Pd(II) and Ag(I) are obtained. Solvent molecules and counter anions fill voids close to the silver cations; more weakly coordinating anions are engaged in longer, the triflate anion in a shorter interaction to Ag(I). In contrast to powder samples, larger crystals of these one-dimensional polymers are rather stable with respect to desolvation. Two isomorphous 1D structures undergo a fully reversible *k*₂ phase transition which can be monitored by single crystal diffraction. The phase transition temperature depends on the nature of the counter anion and may therefore be tuned as a function of chemical composition. The formation of chain polymers by linking Pd(acacCN)₂ building blocks with Ag(I) salts of BF₄⁻, ClO₄⁻, PF₆⁻ and CF₃SO₃⁻ follows chemical intuition whereas its reaction with silver nitrate leads to an unexpected and close-packed 3D structure in which layers of composition Ag(NO₃) are connected by Pd(acacCN)₂ linkers.

1 Introduction

The structural chemistry of coordination polymers has attracted wide interest over the last decades: Many cations may act as potential coordination centers, and they can be interconnected by a wide range of electronically and geometrically different ligands. The resulting solids often show tunable^{1,2} and useful properties, *e.g.* for applications in gas storage,^{3–5} separation,⁶ optics,⁷ or magnetochemistry.⁸

Bimetallic coordination polymers, *i.e.* extended solids based on the regular arrangement of more than one type of cation, offer additional challenges for synthesis and potential for application. Among the linkers for such bimetallic systems, substituted acetylacetonates (acac) have been particularly successful. Two obvious reasons for this success shall shortly be mentioned: The chelating nature of the acetylacetonate moiety conveys additional stability to metal coordination by this group of the ditopic linker, and the different

Pearson hardnesses⁹ of the potential coordination sites favour crosslinking of different cations without disorder. Four examples of ditopic Hacac derivatives have been compiled in Scheme 1.



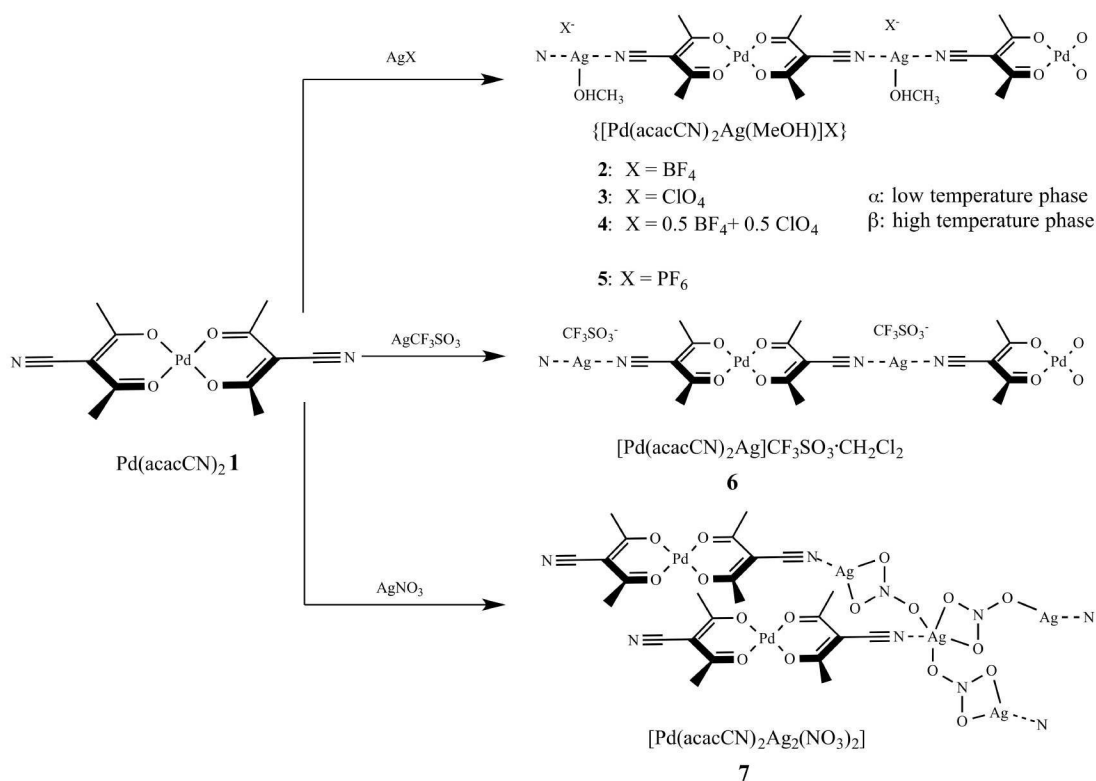
Scheme 1 Examples of ditopic Hacac derivatives.

O,O' coordination by the chelating acac moiety is possible in all these ligands. In addition, the pyridine derivatives in Scheme 1 (ligands a–c) behave as good N nucleophiles to metal cations. This was confirmed in reports about the coordination chemistry of the mono-pyridyl ligands a^{10–14} and b,¹⁵ and of the di-pyridyl derivative c.^{16,17} 3-(4-pyridyl)-acetylacetonate (Scheme 1, a) has also been employed in halogen- and hydrogen-bonded extended structures.¹⁸ In contrast, the N donor capabilities of the nitrile-substituted 3-cyanoacetylacetonate HacacCN (Scheme 1, d) are much less pronounced. Earlier work with this ligand has covered the *O,O'* coordination chemistry of Cu, Fe,¹⁹ Cr,²⁰ Al,²¹ and rare earth cations.^{22,23} All previous examples with the exception of

[†] Electronic Supplementary Information (ESI) available: [Crystallographic information in CIF format, displacement ellipsoid plots for 1–7, powder patterns for 2, 3, 5 and 7, Intensity ratio *I*(*h*/*k*/*l*) for 2 and 3 over larger temperature ranges, Intensity of single reflections in 2, 3 and 4, ¹⁹F NMR result of 4 and sequence of slides visualizing the phase transition in 2.]. See DOI: 10.1039/b000000x/

^a Institute of Inorganic Chemistry, RWTH Aachen University, Aachen, Germany. Fax: +49-241-8092288; Tel: +49-241-8094666; E-mail: ullrich.englert@ac.rwth-aachen.de

^b Carleton College, 300 North College Street, Northfield, MN, USA. Tel: +1-612-8021080; Email: sir@carleton.edu.



Scheme 2 Synthesis and composition of the building block, **1**; and the bimetallic polymeric solids, **2-7**.

a Cu-Ag bimetallic ladder structure involve coordination numbers of at least 6 at the cations;¹⁹ no square-planar complexes based on acacCN have been structurally characterized to date, although this coordination mode has been encountered for the unsubstituted parent ligand acac and several of its substitution products.^{24–26}

In this contribution, we report the synthesis and characterization of the square-planar complex $\text{Pd}(\text{acacCN})_2$, **1**, and its use as a building block for bimetallic extended solids based on Pd(II) and Ag(I) cations. Scheme 2 summarizes our results. Given the linear disposition of the peripheral N donor sites in **1** and the general preference of Ag(I) centers for linear coordination, too, the formation of chain polymers **2-6** is no surprise. The fully reversible and structural phase transition in one of these structure types leads to an unpredicted tunable property, and the 3D network **7** represents a less intuitive way for combining its constituents.

2 Results and Discussion

2.1 Description of the Crystal Structures

The square planar building block $\text{Pd}(\text{acacCN})_2$, **1**, has been obtained by reaction of the ligand HacacCN with palladium

acetate and an auxiliary base in a mixture of water and methanol applying a rather long reaction time of 16 hours. The building unit is obtained as phase pure yellow microcrystalline powder and can be recrystallized from acetone or THF under formation of yellow needle-shaped crystals.

1 crystallizes in the triclinic space group $P\bar{1}$ with the central palladium cation located on an inversion center. The substituted acetylacetonate deviates only slightly from ideal planarity with the nitrogen atom of the nitrile group 0.034 Å dislocated from the plane defined by palladium and the two coordinating oxygen atoms. For reasons of symmetry, the palladium center and its four coordinating oxygen atoms are exactly coplanar. The coordination environment around the metal features an intra-ligand O-Pd-O bite angle of $94.30(7)^\circ$ and a *cis* inter-ligand angle of $85.70(7)^\circ$. In crystalline **1**, the molecules are arranged in parallel stacks. Each building unit within the stacked layers is displaced by the length of the *a* axis with respect to the next neighboring molecule resulting in close contacts between the carbon atom C3 of each molecule and the Pd atom of the neighboring molecules along the stacking direction. The $\text{Pd1}^i \cdots \text{C3}$ distance amounts to 3.282(3) Å. Stacking of the molecules and the molecular packing as space filling model is presented in Fig. 1. A similar stacking pattern was described for the unsubstituted $\text{Pd}(\text{acac})_2$ complex.²⁶

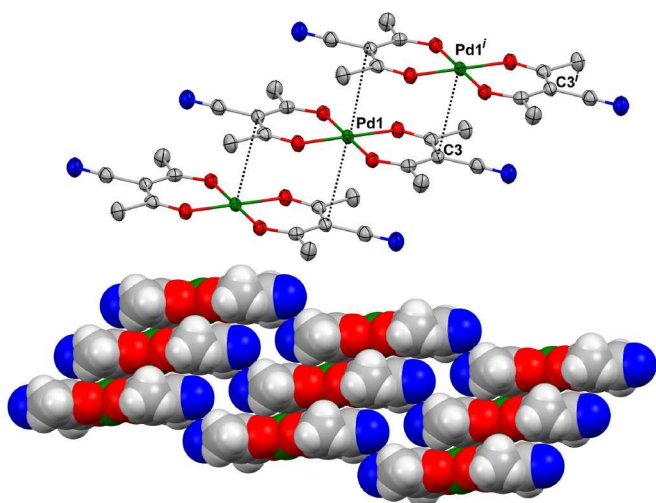


Fig. 1 Intermolecular contacts between Pd1^{*i*} and C3 within the stacking layers and space filling model of the molecular packing. Ellipsoid are drawn at 75 % probability level. Symmetry operation: $i = -1+x, y, z$.

comp.	chain direction	Pd...Pd (intra, Å)	Ag...Pd...Ag (deg)	Pd...Pd (inter, Å)
2α	[1 0 -1]	15.8275(14)	179.13(2)	4.5849(6)
3α	[1 0 -1]	15.8403(3)	179.40(2)	4.6068(8)
5	[1 -1 -1]	15.790(7)	176.32(2)	4.818(2)
6	[1 0 -1]	15.769(2)	180.0	4.9592(6)

Table 1 Comparison of intra- and interchain parameters in **2-6**.

The building block **1** features two uncoordinated nitrile groups with linear NC...Pd...CN arrangement. By addition of silver salts, these weak donor sites may be crosslinked via Ag(I) cations to infinite chains. In contrast to the individual constituents, the resulting bimetallic derivatives **2-7** are much less soluble in common solvents and directly precipitate from solutions of the required stoichiometry. N coordination of a silver ion results in a significant shift in the IR resonance associated with the C-N triple bond to higher wavenumbers.²³ In the chain polymers **2-6**, Pd building blocks and Ag(I) cations are arranged in an alternating sequence, thus forming one-dimensional cationic scaffolds with the counterions included in voids of the crystal structures, in direct neighborhood of the Ag(I). A comparison of intra- and interchain parameters is provided in Table 1.

Compounds **2-5** are methanol solvates. **2** and **3** are isomorphous and show a phase transition at low temperature (see Section 2.2, Tunable Phase Transition); for easier comparison, the following discussion will address the low temperature α phases. In order to study the relationship between chemical composition and phase transition temperature, we prepared

comp.	Ag-N (Å)	N-Ag-N (deg)	Ag...O (methanol, Å)	Ag...X (anion, Å)
2α	2.135(4), 2.135(4)	175.74(13)	2.573(3)	2.716(3) (X=F)
3α	2.134(2), 2.138(2)	178.70(10)	2.598(2)	2.762(2) (X=O)
4α	2.126(5), 2.133(5)	175.5(2)	2.567(5)	2.710(4) (X=0.5F+0.5O)
5	2.100(7), 2.105(7)	169.8(3)	2.551(9)	2.807(11) (X=F)

Table 2 Details concerning Ag(I) coordination in **2-5**.

the mixed crystal **4**, also isomorphous to **2** and **3**. **5** adopts a crystallographically different but topologically equivalent solvate structure. As an example, a section of the polymer chain in the crystal structure of **2 α** is shown in Fig. 2. Fig. 2 also shows the Ag(I) environment in the solids **2 α -5**: each cation adopts a 2 + 1 + 1 coordination. In addition to its almost linear coordination by two nitrile N atoms in direction of the polymer chain, a significantly longer interaction with a methanol oxygen exists perpendicular to the strand. On the opposite side of the polymer, the counter anion resides; its closest contact to the Ag(I) cation is still within the commonly accepted van der Waals radii. The 4 atoms interacting with the silver cation are almost coplanar. Table 2 summarizes the details concerning Ag(I) coordination.

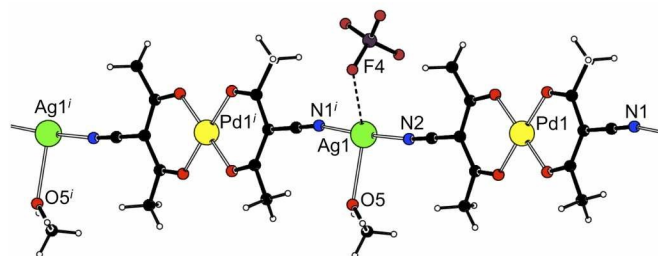


Fig. 2 Section of a polymer chain in **2 α** and 2 + 1 + 1 coordination of the Ag(I) cation; the situation in **3 α** , **4 α** and **5** is similar. Symmetry operator $i = x+1, y, 1-z$.

Chain polymer **6** is a CH₂Cl₂ solvate. Its essentially linear coordinated Ag(I) cations prefers a secondary interaction with the counteranion triflate. This behavior does not only reflect the less pronounced donor capabilities of the solvent but is also in agreement with results from Mak and Chen,²⁷ who state in a more general context that triflate acts as a more coordinating counteranion than BF₄⁻, ClO₄⁻ or PF₆⁻. The asymmetric unit of **6** contains two symmetrically independent Pd(II) cations situated on crystallographic centres of inversion as well as two acacCN ligands, an Ag(I) cation, a triflate anion and a solvent molecule in general position; in line with these

symmetry requirements, coordination of the anion to silver occurs from alternating sides of the polymer strand, *cf.* Fig. 3.

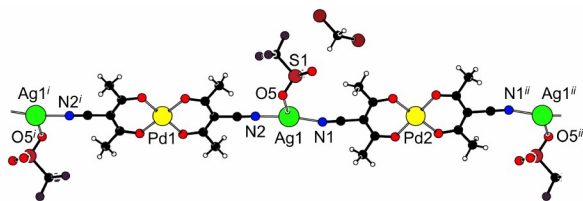


Fig. 3 Section of a polymer chain in **6**; $i = -1-x, 2-y, 1-z$; $ii = 2-x, 2-y, -1-z$.

Classical hydrogen bonds in **2 α -5** only occur along the chains and are entirely absent in **6**. The individual polymer strands in **2 α -6** only weakly interact without specific short interchain contacts. Fig. 4 shows the packing in **2 α** along the chain direction: stacking of cationic polymers precludes highly efficient space filling. We will come back to this point in the context of the packing discussion of **7**.

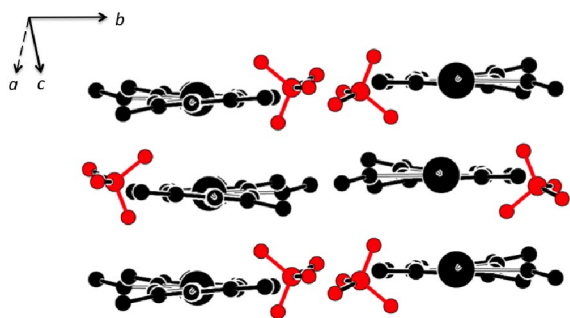


Fig. 4 Projection of **2 α** in the direction of the polymer chains, along $[1\ 0\ -1]$; cationic chains are shown in black, BF_4^- counter anions in red.

2 α -5 are moderately stable, **6** rather unstable towards desolvation. Larger single crystals may easily be recovered from the mother liquor and handled in air for minutes. Grinding of the samples for powder diffraction results in crystalline solids; their powder patterns, however, do not match the simulation based on the single crystal structures. When solid samples of **2 α** , **3 α** and **5** are freshly isolated, hardly ground and subjected to powder diffraction while still moist, the powder pattern of the bulk is in agreement with the expectation from the single crystal structure. The corresponding powder patterns for these solids are shown in the ESI (Figs S9, S10 and S11). The moderately fast desolvation also causes problems in elemental analyses of the bulk; in the case of **5** removal of the solvent seems to be incomplete. In contrast, we have not been able to obtain a powder pattern for **6** which matches its single crystal structure; shortly after removal from the mother liquor,

isolated material already corresponds to the solvent-free compound as shown by elemental analysis, *cf.* 4.2.3.

In contrast to the chain polymers discussed above, compound **7** forms a 3D network: Neutral layers of the composition $[\text{AgNO}_3]_n$ extend in the crystallographic ac plane, and $\text{Pd}(\text{acacCN})_2$ building blocks oriented along the b axis connect these layers in the third dimension as shown in Fig. 5.

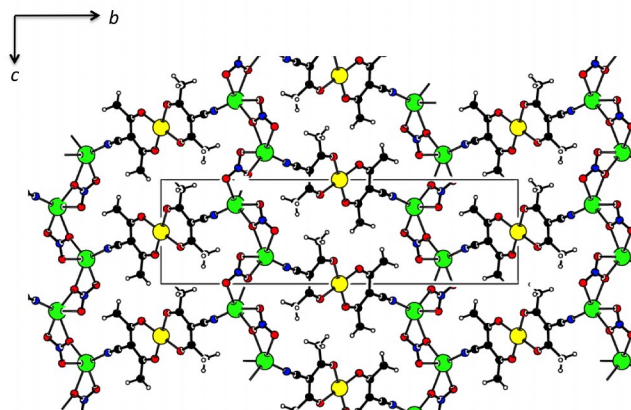


Fig. 5 3D network in the crystal structure of **7**.

The silver coordination in **7** differs significantly from that in the chain polymers: each Ag cation is coordinated by only one acacCN nitrogen atom and by four oxygen atoms of three different nitrate groups. In agreement with the layer stoichiometry, each nitrate coordinates three different cations, one of them in a chelating fashion. The coordination around a cation and that of a nitrate anion are shown in Fig. 6.

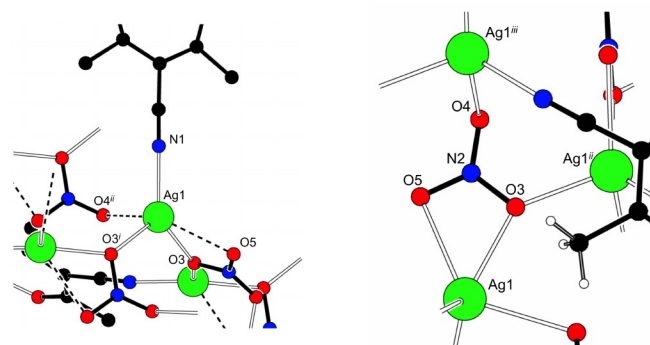


Fig. 6 Coordination of an Ag(I) cation (left) and an anion (right) in the crystal structure of **7**; $i = 3-x, -y, 1-z$; $ii = x, 0.5-y, z-0.5$; $iii = x-1, 0.5-y, z-0.5$.

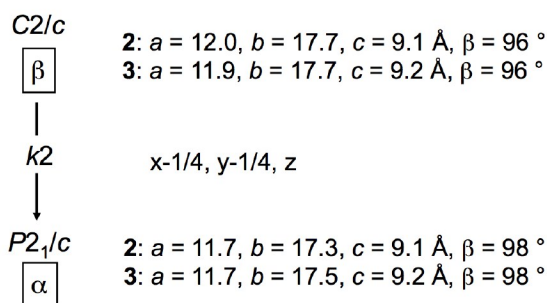
The coordination polyhedron around silver may be described as a distorted square pyramid, with N1 at the apex and the oxygen atoms in the basal plane. The distortion is reflected in the fact that the Addison τ ²⁸ and the Holmes²⁹ parameter do not agree with respect to the idealized polyhedron:

The former amounts to 0.03 and hence almost the ideal value for square-pyramidal coordination whereas the latter indicates 41% of square-pyramidal character on the Berry pseudo rotation path towards trigonal-bipyramidal coordination. Space filling in **7** (fraction of occupied versus total volume³⁰ 0.747) is more efficient than in the chain polymers **2-5** (0.705 - 0.708) or in the molecular compound **1** (0.716). We also emphasize that our 3D coordination polymer **7** is obtained as a phase pure product: Fig. S12 (in the ESI) shows the powder pattern of the bulk as synthesized and the calculated pattern based on the single crystal X-ray diffraction experiment. A few examples³¹⁻³⁶ involving nitrate anions which coordinate three Ag cations have been documented in the CSD.^{37,38}

2.2 Tunable Phase Transition

With respect to topology, **2** and **3** are related to the other chain polymers; their structure corresponds to chemical intuition. During bulk characterization of these compounds, we detected discrepancies between their crystal structures at 100 K and room temperature. We will shortly explain the relationship between low- and high temperature phases: According to the symmetry principle,³⁹ the symmetry relationship between solids before and after a structural phase transition can be described with the help of group theory. For a detailed overview about the concepts in the following discussion, we refer to the excellent monography by Müller.⁴⁰ In a second order phase transition, cooling of a high temperature form results in a phase of lower symmetry. The new phase either adopts a translationengleiche (*t*) or klassengleiche (*k*) subgroup of the original space group. If the phase transition starts from a single crystal, a *t* phase transition will give a twin, with the twin domains related by the symmetry element missing in the subgroup. Twins of this kind are often easy to detect by diffraction experiments. In contrast, a *k* phase transition produces antiphase domains; their diffraction pattern can in general not be distinguished from that of a single crystal. Phase transitions of the *k* type are not readily detected by diffraction; the transition may show up in thermal analysis but the enthalpy associated with a second order phase transition may be small. In the field of molecular crystals, we are aware of earlier work by Guzei *et al.*^{41,42} and of a temperature-dependent study concerning tris(acetylacetonato) complexes of aluminium⁴³ and chromium.⁴⁴ We have encountered this situation for the isomorphous chain polymers **2** and **3**; Scheme 3 shows the symmetry relation between their phases.

As **2** and **3** are isomorphous but differ in the phase transition temperature, we also prepared the solid solution **4**. For this compound, the combination of tentative occupancy refinements based on diffraction data (see 4.3) and NMR results (see 4.2.2) suggests statistical disorder of the counter anions BF_4^- and ClO_4^- in equimolar ratio. We can thus



Scheme 3 Symmetry relationship between the high (β) and low (α) temperature phases of the compounds.

correlate the transition temperature with chemical composition. Temperature-dependent powder diffraction, usually the method of choice for monitoring phase transitions, cannot be applied in the present case because loss of the weakly coordinated methanol molecules leads to decomposition and formation of structurally different solvent-free compounds. Fortunately, larger single crystals are much more inert with respect to desolvation and even allow for data collection times of several hours at elevated temperatures, *e.g.* 320 K. Therefore, analysis of the phase transition in each solid required several full intensity data collections in the proximity of its transition temperature; these experiments also unambiguously confirmed that the phase transition is fully reversible. Details are given in the Experimental Part.

We will first focus on the effects of the phase transition in real space. In the low temperature α phases, all atoms reside in general position in space group $P2_1/c$, with a complete formula unit of the chain polymer in the asymmetric unit. As an example, the geometry for 2α is discussed here; the situation in the low temperature forms of **3** and **4** is very similar. The Ag(I) cation is coordinated by two nitrile groups at short distances (*ca.* 2.1 Å) in an almost linear fashion (N1-Ag1-N2i = 175.75(15) Å). Additional interactions involve close contacts to a solvent methanol molecule (Ag1-O5 = 2.573(4) Å) and to a tetrafluoroborate anion (Ag1-F4 = 2.716(3) Å). In the other compounds, perchlorate (**3**) or a mixture of tetrafluoroborate/perchlorate with statistical occupancy (**4**) act as counteranions. Angles involving the longer contact distances, *e.g.* O-Ag-N, show that the overall Ag environment is asymmetric (Fig. 7 bottom).

In the high temperature β phases, the chain polymers adopt space group $C2/c$ with Pd(II) and Ag(I) on crystallographic twofold axes. Consequently, the asymmetric unit comprises only half a formula unit of the polymer. The resulting local environment about Ag(I) (Fig. 7 top) exhibits very similar values for the short Ag-N distances and the subtended angle as in the α phase. It is, however, necessarily symmetric,

and the metal cations are precisely aligned when viewed in the direction of chain propagation, *i.e.* along [1 0 -1]. Symmetry in the β phases involves disorder of the coordinated methanol molecules about the crystallographic twofold axis passing through the Ag(I) center.

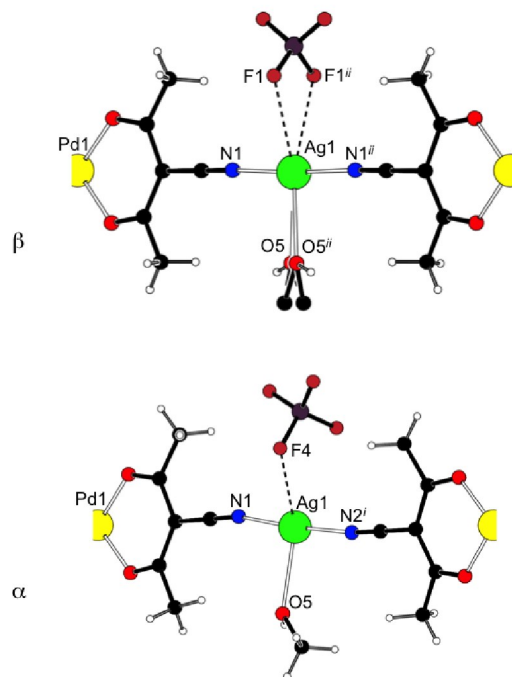


Fig. 7 Local environment about the Ag(I) cations in the β (top) and α (bottom) phase of **2**; view direction is along [0 0 1]. The situation for **3** and **4** is similar. Symmetry operators: $i = x+1, y, z-1$; $ii = 2-x, y, 0.5-z$.

How about reciprocal space? The C centering of the unit cells associated with the high temperature β forms implies the integral reflection condition $hkl, h+k = 2n$. Reflection intensities for $hkl, h+k = 2n+1$ should be systematically absent. With respect to the overall diffraction pattern, the ratio between the latter forbidden and the former allowed reflection intensities, expressed as

$$I(f/t) = \frac{\sum I_{(h+k=2n+1)}}{\sum I_{(h+k=2n)}} \quad (1)$$

should assume very small values, ideally zero, at the phase transition temperature. The ab plane with its C centering for the high temperature phases is shown in Fig. 8a.

For the low temperature α phases, no integral reflection condition can be expected. Fig. 8b shows, however, that the arrangement of the most relevant scattering centers in the α phases is rather similar to that in β : pronounced pseudosymmetry is observed, and therefore the intensity of reflections $hkl, h+k = 2n$ exceed those of $hkl, h+k = 2n+1$ significantly,

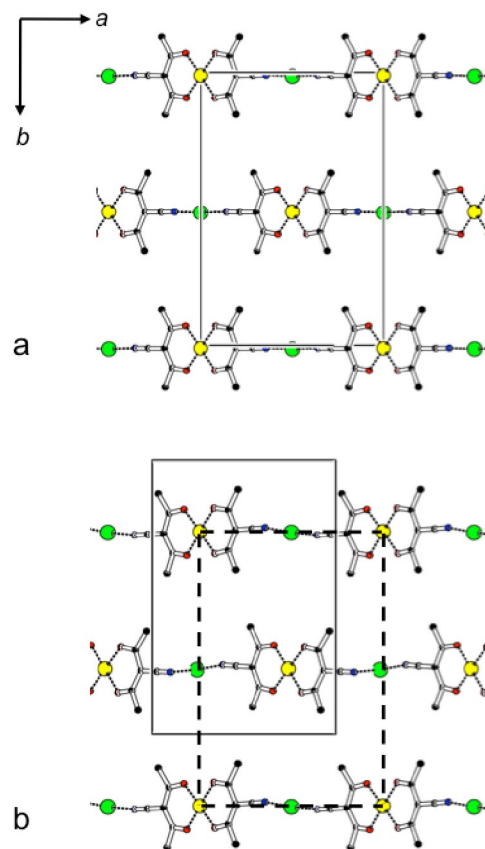
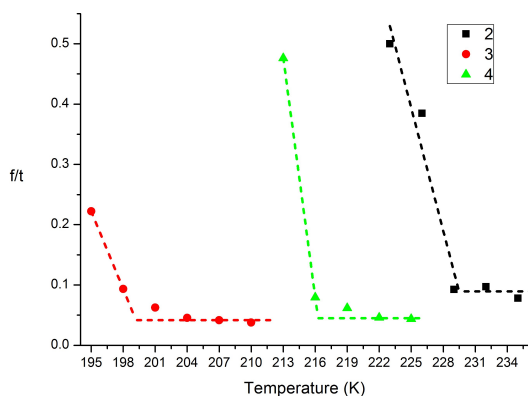


Fig. 8 Projections of the C -centered β phase (a) and the pseudo-centered α phase (b) of **2**; conventional unit cells are indicated by solid, the centered pseudo-cell for 2α by dashed lines. H atoms, coordinated methanol and BF_4^- anions have been omitted for clarity; the situation in **3** and **4** is similar.

evenly, even below the phase transition temperature. This fact was indeed the original motivation for temperature-dependent diffraction experiments on crystals of **2** which ultimately led to the discovery of the phase transition. Even at 100 K, far away from the phase transition temperature, reflections with $h+k = 2n$ are much stronger than those not matching this condition, and hence the corresponding value for $I(f/t)$ in eq. 1 amounts to ca. 0.5. Obviously, for any structure without pseudosymmetry, a ratio close to unity is expected. In agreement with the requirements for the order parameter⁴⁰ in a second order phase transition, the intensity ratio $I(f/t)$ calculated according to eq. 1 is a function of temperature in the low symmetry form; it approaches a small value at the phase transition and remains close to zero in the high symmetry phase. Remarkably, the isomorphous solids **2** and **3** differ significantly in their phase transition temperatures; Scheme 4 summarizes these results.

Due to relatively fast desolvation of powder samples, our



Scheme 4 Intensity ratio $I(f/t)$ as a function of temperature for **2**, **3** and the mixed anion compound **4**.

experiments have been conducted on larger and more stable single crystals. Each individual data point specifies an $I(f/t)$ ratio at a given temperature and is based on a complete set of intensity data. In the context of these experiments, we did not only obtain information concerning the transition temperatures but we could also confirm the expectation that the phase transitions are fully reversible and that single crystals can survive even after five consecutive cycles of heating and cooling.

2 and **3** share the same cationic chain polymer structure but differ with respect to their counter anions. The difference in their phase transition temperatures encouraged us to test whether this property might be tuned by chemical substitution in the anionic part of the structure. We had encountered an analogous example for the t_2 phase transition in the one-dimensional polymers $[\text{Cd}(\mu\text{-X})_2\text{py}_2]$ ($\text{X} = \text{Cl}, \text{Br}; \text{py} = \text{pyridine}$).¹ A chain polymers in which tetrafluoroborate and perchlorate occupy the anion positions in statistical distribution can indeed be prepared: This molecular alloy **4** is also isomorphous with **2** and **3**, crystallizing in the same space group with similar lattice parameters. Tentative refinement of the atomic site occupancies in the anion region unambiguously proved the concomitant presence of tetrafluoroborate and perchlorate. In the final refinement of the low temperature intensity data for **4** α , the anion site was treated as equally populated by both alternative anions; additional details are provided in section 4. Coordination polymer **4** also meets the expected property with respect to the k_2 phase transition and features an intermediate transition temperature as shown in Scheme 4. In view of the fact that intensity data collected at 320 K, *i. e.* well above the phase transition temperatures, showed large anisotropic displacement parameters for the individual anions in **2** and **3**, no attempt was made to establish a disorder model with atomic resolution for the high temperature form **4** β .

3 Conclusion

Crosslinking of the new building block $\text{Pd}(\text{acacCN})_2$, **1**, with silver salts leads to products of two topologies. In **2-6**, the alternating arrangement of neutral $\text{Pd}(\text{acacCN})_2$ units and $\text{Ag}(\text{I})$ cations results in cationic chains, with counteranions and solvent molecules close to the silver. In the alternative 3D network **7**, $\text{Pd}(\text{acacCN})_2$ bridges $[\text{AgNO}_3]_n$ layers. In contrast to the less coordinating anions BF_4^- or PF_6^- , nitrate is well-known to coordinate to $\text{Ag}(\text{I})$: both chelating and bridging geometries occur with quite high frequency. A search in the Cambridge Structural Database^{37,45} revealed 721 entries in which a nitrate anion is coordinated to silver. In 274 of these cases, a chelating NO_3 coordination to Ag was observed, and in 261 entries a nitrate was found bridging between at least two silver centers. 120 crystal structures combine both chelating and bridging nitrate moieties. Future work will be devoted to synthesize and understand more structures featuring AgNO_3 layers.

Our interest is not limited to static crystal structures: The chain polymers **2-4** provide a beautiful example for a k_2 phase transition which may be tuned by chemical substitution. Furthermore, they convey a more general message: A solid studied in a routine diffraction experiment at a single (low) temperature may well be the result of an undetected k phase transition. In the case of **2**, pseudosymmetry has been the key indicator which stimulated additional diffraction experiments at variable temperature, and pseudo symmetry may readily be detected. Pseudosymmetric structures may be retrieved in real space, *e. g.* by screening 3D coordinates available from data bases, or in reciprocal space, by comparing the intensities for different classes of reflections. Our future work will focus on the former approach.

4 Experimental Part

4.1 Materials and Methods

The HacacCN ligand was prepared according to the literature method by Silvernail *et al.*⁴⁶ All chemicals were used without further purification: Palladium acetate (Acros Organics), NaHCO_3 (99.5%, KMF Laborchemie), NaF (99%), NaI (AppliChem), D_2O (99.9%, Aldrich), AgPF_6 (98%, Aldrich), AgCF_3SO_3 (98%, Acros Organics), AgClO_4 (Alfa Aesar), AgBF_4 (98%, Aldrich), and AgNO_3 (99.5%, Fluka Chemie).

IR spectra were recorded on a Nicolet Avatar 360 E.S.P. spectrometer in KBr windows for **1** and in nujol mull for **2**, **3**, **5** and **7**. CHN microanalyses were carried out at the Institute of Organic Chemistry, RWTH Aachen University, using a HERAEUS CHNO-Rapid. Powder diffraction experiments were performed at room temperature on flat samples with a Stoe & Cie STADI P diffractometer equipped with an image-

plate detector with constant ω angle of 55° using germanium-monochromated Cu- $K_{\alpha 1}$ radiation ($\lambda = 1.54051 \text{ \AA}$).

4.2 Syntheses

4.2.1 Synthesis of Pd(acacCN)₂, 1. HacacCN (250 mg, 2 mmol) was dissolved in a mixture of MeOH/H₂O (2 mL/7 mL). NaHCO₃ (168 mg, 2 mmol) was slowly added (20 min). Palladium acetate (224 mg, 1 mmol) was suspended in the solution of the deprotonated ligand. The suspension was stirred for 16 hours at 35°C . After two hours formation of a yellow solid started. After sixteen hours the yellow precipitate was filtered (G3 frit with pore size of *ca.* 20-40 microns), washed with water, and dried in a desiccator. Yield: 253 mg (0.71 mmol, 71%). Recrystallization from acetone allowed the growth of suitable single crystals. Analysis: CHN: Anal. Calcd. for [Pd(acacCN)₂]: C₁₂H₁₂PdN₂O₄: C: 40.64, H: 3.41, N: 7.90. Found: C: 40.32, H: 3.38, N: 7.85. IR: $\nu(\text{C}\equiv\text{N}, \text{cm}^{-1}) = 2210$.

4.2.2 Syntheses of [Pd(acacCN)₂Ag(MeOH)]BF₄, 2, [Pd(acacCN)₂Ag(MeOH)]ClO₄, 3, [Pd(acacCN)₂Ag(MeOH)]0.5BF₄·0.5ClO₄, 4 and [Pd(acacCN)₂Ag(MeOH)]PF₆, 5. The building unit **1**, (18 mg, 0.05 mmol) was dissolved in 3 mL CH₂Cl₂. AgBF₄ (9 mg, 0.05 mmol) was dissolved in 3 mL methanol and layered above it with an intermediate layer of 1 mL CH₂Cl₂ and 1 mL methanol. Yellow crystals were obtained after one week of crystallization time and single crystal X-ray diffraction characterized them as the linear chain polymer **2a**. Yield: 14 mg (0.025 mmol, 50%) Analysis: CHN: Anal. Calcd. for [Pd(acacCN)₂AgBF₄]: C₁₂H₁₂AgBF₄N₂O₄Pd: C: 26.24, H: 2.20, N: 5.10. Found: C: 26.16, H: 2.70, N: 4.76. IR: $\nu(\text{C}\equiv\text{N}, \text{cm}^{-1}) = 2237$.

The analogous reaction conducted with AgClO₄ (10 mg, 0.05 mmol) and AgPF₆ (13 mg, 0.05 mmol) as cross-linking reagent yielded the chain polymers **3** and **5**, respectively. Yield for **3**: 15 mg (0.027 mmol, 54 %) Analysis: CHN: Anal. Calcd. [Pd(acacCN)₂AgClO₄]: C₁₂H₁₂AgClN₂O₈Pd: C: 25.65, H: 2.15, N: 4.98. Found: C: 25.87, H: 2.47, N: 4.80. IR: $\nu(\text{C}\equiv\text{N}, \text{cm}^{-1}) = 2229$. Yield for **5**: 16 mg (0.026 mmol, 52%) Analysis: CHN: Anal. Calcd. for [Pd(acacCN)₂AgPF₆]: C₁₂H₁₂AgF₆N₂O₄PPd: C: 23.72, H: 1.99, N: 4.61. Found: C: 24.54, H: 2.41, N: 4.55. IR: $\nu(\text{C}\equiv\text{N}, \text{cm}^{-1}) = 2237$.

For the more complex case of the mixed crystals **4**, in a test tube, the building block Pd(acacCN)₂ (0.018 g, 0.05 mmol) was dissolved in 3 mL CH₂Cl₂. A solvent mixture of 0.10 mL CH₂Cl₂ and 0.10 mL CH₃OH was used as an intermediate layer, and a solution of AgBF₄ (0.008g, 0.04 mmol) and AgClO₄ (0.002g, 0.01 mmol) in 1 mL CH₃OH was layered on top. After 2 days, yellow crystals of **4** were obtained. The composition of these mixed crystals with respect to the anion content was determined by site occupancy refinement (see

section 4.3) and controlled by ¹⁹F NMR spectroscopy. For this purpose, a known quantity of **4** was decomposed by addition of NaI in D₂O; after separation from the precipitated AgI, a solution of NaF in D₂O was added as internal standard. Integration of the ¹⁹F resonances suggested a BF₄⁻ content of *ca.* 0.4 per Ag(I) cation.

Single crystals of **2-5** are stable for a limited amount of time after they have been removed from the reaction mixture. Grinding of the products for powder diffraction studies showed rapid loss of the coordinated methanol molecules for all three structures. Therefore all yield calculations and theoretical CHN values refer to the solvent free compounds.

4.2.3 Synthesis of [Pd(acacCN)₂Ag]CF₃SO₃·CH₂Cl₂, 6. The building unit **1**, (18 mg, 0.05 mmol) was dissolved in 3 mL CH₂Cl₂. AgCF₃SO₃ (13 mg, 0.05 mmol) was dissolved in 3 mL of methanol and layered on top of an intermediate layer of 2mL CH₂Cl₂ Yellow crystals were obtained after one week of crystallization time and single crystal X-ray diffraction characterized them as the linear chain polymer **6**. Crystals lose their crystallinity within minutes when they are removed from the reaction mixture. For CHN analysis and yield calculation crystals were dried in vacuum, and calculated values refer to the solvent free compound. Yield: 18 mg (0.029 mmol, 58%) Analysis: CHN: Anal. Calcd. for [Pd(acacCN)₂AgCF₃SO₃]: C₁₃H₁₂AgF₃N₂O₇PdS: C: 25.53, H: 1.98, N: 4.58. Found: C: 24.89, H: 2.13, N: 4.04.

4.2.4 Synthesis of [Pd(acacCN)₂Ag₂(NO₃)₂], 7. The building unit **1**, (18 mg, 0.05 mmol) was dissolved in 3 mL CH₂Cl₂. AgNO₃ (16 mg, 0.10 mmol) was dissolved firstly in one drop of water and then 3 mL of methanol were added. The solution was layered on top of the building unit solution with an intermediate layer of 1 mL CH₂Cl₂ and 1 mL methanol. Yellow crystals were obtained after one day of crystallization time and they were identified by single crystal X-ray diffraction as 3D network **7**. Crystals are stable after they have been removed from the reaction mixture. Yield: 19 mg (0.028 mmol, 56%) Analysis: CHN: Anal. Calcd. for [Pd(acacCN)₂Ag₂(NO₃)₂]: C₁₂H₁₂Ag₂N₄O₁₀Pd: C: 20.76, H: 1.74, N: 8.07. Found: C: 20.73, H: 1.80, N: 8.08. IR: $\nu(\text{C}\equiv\text{N}, \text{cm}^{-1}) = 2233$.

4.3 Crystallographic Studies

The diffraction experiments were performed with a Bruker D8 goniometer equipped with an Incoatec microsource (Mo- K_{α} , $\lambda = 0.71073 \text{ \AA}$, multilayer optics) and an APEX CCD detector; the sample temperature was controlled with an accuracy of *ca.* 2 K with an Oxford Cryostream 700 instrument. Intensity data were integrated with SAINT⁴⁷ and corrected for absorption by multi-scan methods using the program SADABS.⁴⁸

Details about the structure models are given at the end of this section; we first describe the temperature-dependent diffraction experiments for establishing the phase transition temperatures. Powder diffraction would usually be the method of choice and much faster; powder samples of the coordination polymers **2-4**, however, undergo fast desolvation of co-crystallized methanol, and reliable powder patterns can only be obtained on moist samples for a short period. All diffraction data have therefore been collected on single crystals which proved considerably more stable towards solvent evaporation. For each compound, a subset of intensity data was collected at intervals of 15 K to roughly determine the transition temperature. Close to the phase transition, complete intensity data sets were collected according to nested intervals above and below the transition temperature in 3 K steps. In this way, the phase transition temperature could be determined with reasonable accuracy and at the same time the reversibility of the transition could be proven.

The crystal structures were solved with Patterson or Direct methods, and refinements were accomplished with full matrix least-square procedures as implemented in SHELXL-13.⁴⁹ All non-hydrogen atoms were assigned anisotropic displacement parameters; hydrogen atoms were placed in idealized positions and included as riding with constrained isotropic displacement parameters. In **2**, **3**, **4** and **5**, the hydrogen atoms of the hydroxyl group of the methanol molecule were located as electron density maxima from the Fourier difference maps and included in the refinement with distance restraints.

For compounds **2-4**, the data collection temperatures of 100 and 320 K were well below or above the phase transitions temperatures, and assignment of the space groups was unambiguous. In **3 α** , two oxygen atoms of the perchlorate anion showed positional disorder. The occupancy of two alternative positions was refined using distance restraints; it converged at a 40:60 ratio for the alternative orientations. In the case of **4**, tentative refinements allowed to exclude simple BF₄⁻ or ClO₄⁻ models for the anion; treatment of this site as substitutionally disordered by both moieties, with constrained coordinates and anisotropic displacement parameters, suggested a slight (60:40) preference of tetrafluoroborate over perchlorate. In view of the correlation between displacement parameters and site occupancies and the potential bias introduced by constraining F (in BF₄⁻) and O (in ClO₄⁻) to the same coordinates, we undertook an independent analysis based on integration of the ¹⁹F NMR resonances (see above). This experiment confirmed the almost equimolar presence of both anion species but rather suggested a slightly preferential occupancy of the anion site by perchlorate. In the final structure model for **4 α** , the anion as therefore treated as disordered with equal occupancy for tetrafluoroborate and perchlorate, in reasonable agreement with the results of both experimental methods. No attempt was made to obtain a structure model at atomic res-

olution for the (necessarily disordered) β phase of **4** under these conditions. After refinement of the structure model for **5**, the most disagreeable reflections showed a clear tendency for $F^2(\text{obs.}) \gg F^2(\text{calc.})$. A test with the help of the TwinRotMat option in PLATON³⁰ confirmed non-merohedral twinning for this sample, with 1056 out of 7996 reflections overlapping. An appropriately modified set of intensity data taking the partially overlapped diffraction of both domains into account (HKL F5 format in SHELXL97⁵⁰) gave significantly improved convergence results and relative domain fractions of 0.75 and 0.25. One fluorine atom of the PF₆⁻ anion showed positional disorder and the occupancy of two alternative positions was refined converging at a 40:60 ratio. The affected atoms were refined with isotropic displacement parameters.

Acknowledgement

Financial support by China Scholarship Council (Q. G.), DFG (SeleCa) and RWTH Graduiertenförderung (C. M.) are gratefully acknowledged. Paul Müller is gratefully acknowledged for help with powder diffraction experiments.

References

- 1 K. Lamberts, I. Kalf, A. Ramadan, P. Müller, R. Dronskowski and U. Englert, *Polymers*, 2011, **3**, 1151–1161.
- 2 C. Wang, D. Liu and W. Lin, *J. Am. Chem. Soc.*, 2013, **135**, 13222–13234.
- 3 L. L. Welbes and A. S. Borovik, *Acc. Chem. Res.*, 2005, **38**, 765–774.
- 4 D. Banerjee and J. B. Parise, *Cryst. Growth Des.*, 2011, **11**, 4704–4720.
- 5 H. Furukawa, K. E. Cordova, M. O’Keeffe and O. M. Yaghi, *Science*, 2013, **341**, 974.
- 6 K. Kishida, S. Horike, Y. Watanabe, M. Tahara, Y. Inubushi and S. Kitagawa, *Chemistry - An Asian Journal*, 2014, DOI: 10.1002/asia.201400122.
- 7 M.-D. Zhang, H.-G. Zheng, Z.-Z. Liu and X.-Q. Yao, *CrystEngComm*, 2013, **15**, 9265–9275.
- 8 A. Nafady, A. P. O’Mullane and A. M. Bond, *Coord. Chem. Rev.*, 2014, **268**, 101–142.
- 9 R. G. Pearson, *Chemical Hardness. Applications from Molecules to Solids*, Wiley-VCH, Weinheim, 1997.
- 10 V. D. Vreshch, A. N. Chernega, J. A. K. Howard, J. Sieler and K. V. Domasevitch, *Dalton Trans.*, 2003, 1707–1711.
- 11 V. D. Vreshch, A. B. Lysenko, A. N. Chernega, J. A. K. Howard, H. Krautscheid, J. Sieler and K. V. Domasevitch, *Dalton Trans.*, 2004, 2899–2903.
- 12 C. Merckens, K. N. Truong and U. Englert, *Acta Crystallogr. Sect. B*, 2014, **70**, DOI:10.1107/S2052520614006210.
- 13 B. Chen, F. R. Fronczek and A. W. Maverick, *Inorg. Chem.*, 2004, **43**, 8209–8211.
- 14 Y. Zhang, B. Chen, F. R. Fronczek and A. W. Maverick, *Inorg. Chem.*, 2008, **47**, 4433–4435.
- 15 D. Simond, S. E. Clifford, A. F. Vieira, C. Besnard and A. F. Williams, *RSC Adv.*, 2014, **4**, 16686–16693.
- 16 A. D. Burrows, C. G. Frost, M. F. Mahon, P. R. Raithby, C. L. Renouf, C. Richardson and A. J. Stevenson, *Chem. Commun.*, 2010, **46**, 5067–5069.

- 17 A. D. Burrows, M. F. Mahon, C. L. Renouf, C. R. Richardson, A. J. Warren and J. E. Warren, *Dalton Trans.*, 2012, **41**, 4153–4163.
- 18 C. Merckens, F. Pan and U. Englert, *CrystEngComm*, 2013, **15**, 8153–8158.
- 19 A. D. Burrows, K. Cassar, M. F. Mahon and J. E. Warren, *Dalton Trans.*, 2007, **24**, 2499–2509.
- 20 M. Kondracka and U. Englert, *Inorg. Chem.*, 2008, **47**, 10246–10257.
- 21 C. Merckens, N. Becker, K. Lamberts and U. Englert, *Dalton Trans.*, 2012, **41**, 8594–8599.
- 22 C. Merckens and U. Englert, *Dalton Trans.*, 2012, **41**, 4664–4673.
- 23 C. Merckens, O. Pecher, F. Steuber, S. Eisenhut, A. Görne, F. Haarmann and U. Englert, *Z. Anorg. Allg. Chem.*, 2013, **639**, 340–346.
- 24 D. M. Töbrens, M. Hummel, R. Kaindl, H. Schottenberger and V. Kahlenberg, *CrystEngComm*, 2008, **10**, 327–334.
- 25 M. A. G. Berg, M. K. Ritchie and J. S. Merola, *Polyhedron*, 2012, **38**, 126–130.
- 26 M. Hamid, M. Zeller, A. D. Hunter, M. Mazhara and A. A. Tahira, *Acta Crystallogr.*, 2005, **E61**, m2181–m2183.
- 27 X.-D. Chen and T. C. W. Mak, *Chem. Commun.*, 2005, 3529–3531.
- 28 A. W. Addison, T. N. Rao, J. Reedijk, J. van Rijn and G. C. Verschoor, *J. Chem. Soc. Dalton Trans.*, 1984, 1349–1356.
- 29 R. Holmes, *Inorg. Chem.*, 1984, **32**, 119–235.
- 30 A. L. Spek, *Acta Crystallogr.*, 2009, **D65**, 148–155.
- 31 S.-L. Kuang, H.-Y. Li, D.-B. Dang and X.-J. Pan, *Synth. React. Inorg., Met.-Org., Nano-Met. Chem.*, 2012, **42**, 5964.
- 32 T. R. Sarangarajan, B. S. Krishnamoorthy, K. Panchanatheswaran, J. N. Low and C. Glidewell, *Acta Crystallogr.*, 2008, **C64**, m286–m291.
- 33 H. S. Huh, S. Y. Yun and S. W. Lee, *Bull. Korean Chem. Soc.*, 2008, **29**, 1065–1068.
- 34 H. S. Huh, S. H. Kim, S. Y. Yun and S. W. Lee, *Polyhedron*, 2008, **27**, 1229–1237.
- 35 Z.-P. Deng, Z.-B. Zhu, S. Gao, L.-H. Huo, H. Zhao and S. W. Ng, *Dalton Trans.*, 2009, 6552–6561.
- 36 M. H. Shu, C. L. Tu, W. D. Xu, H. B. Jin and J. Sun, *Cryst. Growth Des.*, 2006, **6**, 1890–1896.
- 37 F. H. Allen, *Acta Crystallogr.*, 2002, **B58**, 380–388.
- 38 CSD version 5.35, November 2013, with 658007 entries.
- 39 H. Bärmighausen, *MATCH*, 1980, **9**, 139–175.
- 40 U. Müller, *Symmetriebeziehungen zwischen verwandten Kristallstrukturen*, Vieweg + Teubner, 2011.
- 41 I. A. Guzei, L. C. Spencer, J. W. Su and R. R. Burnette, *Acta Crystallogr.*, 2007, **B63**, 93–100.
- 42 I. A. Guzei, E. M. Gunn, L. C. Spencer, J. M. Schomaker and J. W. Rigoli, *CrystEngComm*, 2011, **13**, 3444–3450.
- 43 L. S. von Chrzanowski, M. Lutz and A. L. Spek, *Acta Crystallogr.*, 2007, **C63**, m129–m134.
- 44 L. S. von Chrzanowski, M. Lutz and A. L. Spek, *Acta Crystallogr.*, 2007, **C63**, m377–m382.
- 45 All numbers in the following analysis refer to error-free structures without disorder.
- 46 C. M. Silvernail, G. Yap, R. D. Sommer, A. L. Rheingold, V. W. Day and J. A. Belot, *Polyhedron*, 2001, **20**, 3113–3117.
- 47 SAINT+ (version 7.68). Program for reduction of data collected on Bruker CCD area detector diffractometer, 2009.
- 48 G. M. Sheldrick, *SADABS (version 2.03). Program for empirical absorption correction of area detector data*, 2004.
- 49 G. M. Sheldrick, *Acta Crystallogr.*, 2015, **C71**, 3–8.
- 50 G. M. Sheldrick, *Acta Crystallogr.*, 2008, **A64**, 112–122.

Compound	1	2α	2β
Temperature (K)	100(2)	100(2)	320(2)
Empirical formula	C ₁₂ H ₁₂ N ₂ O ₄ Pd	C ₁₃ H ₁₆ AgBF ₄ N ₂ O ₅ Pd	C ₁₃ H ₁₆ AgBF ₄ N ₂ O ₅ Pd
Moiety formula	C ₁₂ H ₁₂ N ₂ O ₄ Pd	C ₁₂ H ₁₂ AgN ₂ O ₄ Pd, BF ₄ , CH ₃ OH	C ₁₂ H ₁₂ AgN ₂ O ₄ Pd, BF ₄ , CH ₃ OH
Formula weight (g/mol)	354.64	581.37	581.37
Crystal description	yellow plate	yellow plate	yellow plate
Crystal size (mm)	0.35 x 0.11 x 0.09	0.24 x 0.20 x 0.16	0.26 x 0.22 x 0.26
Crystal system	triclinic	monoclinic	monoclinic
Space group	<i>P</i> $\bar{1}$	<i>P</i> 2 ₁ / <i>c</i>	<i>C</i> 2/ <i>c</i>
<i>a</i> (Å)	4.8536(11)	11.6947(9)	11.9640(16)
<i>b</i> (Å)	7.8906(17)	17.3278(14)	17.688(2)
<i>c</i> (Å)	8.8251(19)	9.1324(7)	9.1080(11)
α (°)	78.1348(27)		
β (°)	86.3966(28)	98.1670(11)	96.437(3)
γ (°)	75.1220(28)		
<i>V</i> (Å ³)	319.65(12)	1831.9(2)	1915.3(4)
<i>Z</i>	1	4	4
μ (mm ⁻¹)	1.462	2.117	2.025
Total/unique reflections	4614/1768	21198/3820	5071/1747
<i>R</i> _{int}	0.0401	0.0597	0.0245
<i>R</i> [<i>F</i> ² > 2 σ (<i>F</i> ²)]	0.0282	0.0418	0.0322
<i>wR</i> ₂ (<i>F</i> ²)	0.0670	0.1242	0.1291
GOF	1.091	1.132	1.000
No. of parameters	90	253	137
$\Delta\rho_{\max}/\Delta\rho_{\min}$ (<i>e</i> Å ⁻³)	0.673/-0.708	1.171 ^a /-1.224 ^b	0.411/-0.515
CCDC	1005519	1005520	1042065

Table 3 Crystal data and refinement results for the square planar building unit Pd(acacCN)₂, **1**, and the bimetallic coordination polymers **2** at 100K and 320K. a: highest peak 1.171 is 1.29 Å from F2; b: deepest hole -1.22 is 0.75 Å from Pd1.

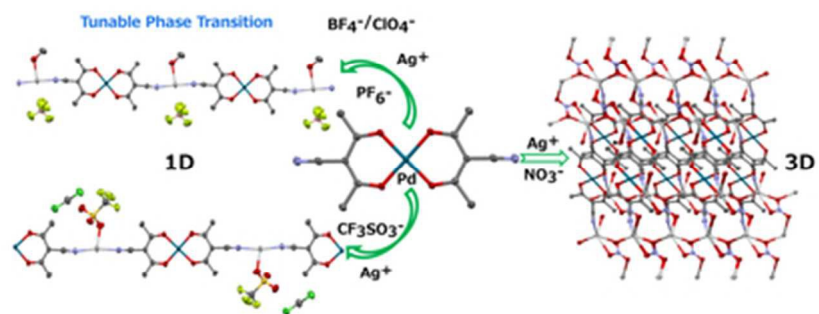
Compound	3 α	3 β	4 α
Temperature (K)	100(2)	320(2)	100(2)
Empirical formula	C ₁₃ H ₁₆ AgClN ₂ O ₉ Pd	C ₁₃ H ₁₆ AgClN ₂ O ₉ Pd	C ₁₃ H ₁₆ AgB _{0.5} Cl _{0.5} F ₂ N ₂ O ₇ Pd
Moiety formula	C ₁₂ H ₁₂ AgN ₂ O ₄ Pd, ClO ₄ , CH ₃ OH	C ₁₂ H ₁₂ AgN ₂ O ₄ Pd, ClO ₄ , CH ₃ OH	C ₁₂ H ₁₂ Ag ₂ N ₂ O ₄ Pd, 0.5BF ₄ , 0.5ClO ₄ , CH ₃ OH
Formula weight (g/mol)	594.02	594.02	587.68
Crystal description	yellow plate	yellow prism	yellow rod
Crystal size (mm)	0.19 x 0.15 x 0.09	0.60 x 0.23 x 0.14	0.29 x 0.17 x 0.17
Crystal system	monoclinic	monoclinic	monoclinic
Space group	<i>P2₁/c</i>	<i>C2/c</i>	<i>P2₁/c</i>
<i>a</i> (Å)	11.7013(18)	11.9150(17)	11.6840(11)
<i>b</i> (Å)	17.518(3)	17.722(3)	17.2956(16)
<i>c</i> (Å)	9.1703(14)	9.1692(13)	9.1223(9)
β (°)	98.006(2)	96.440(2)	98.158(2)
<i>V</i> (Å ³)	1861.4(5)	1924.0(5)	1824.8(3)
<i>Z</i>	4	4	4
μ (mm ⁻¹)	2.211	2.139	2.190
Total/unique reflections	22129/3852	10680/1794	19702/3294
<i>R</i> _{int}	0.0450	0.0508	0.0423
<i>R</i> [<i>F</i> ² > 2 σ (<i>F</i> ²)]	0.0250	0.0359	0.0412
<i>wR</i> ₂ (<i>F</i> ²)	0.0657	0.1194	0.1063
GOF	1.033	0.986	1.060
No. of parameters	272	137	250
$\Delta\rho_{max}/\Delta\rho_{min}$ (e Å ⁻³)	0.759/-0.667	0.659/-1.189 ^c	2.432 ^d /-1.105 ^e
CCDC	1005521	1042066	1042067

Table 4 Crystal data and refinement results for **3** at 100K and 320K as well as **4** at 100K. c: deepest hole -1.189 is 0.74 Å from Ag1; d: highest peak 2.432 is 0.87 Å from Pd1; e: deepest hole -1.105 is 0.53 Å from Cl1.

Compound	5	6	7
Temperature (K)	100(2)	100(2)	100(2)
Empirical formula	C ₁₃ H ₁₆ AgF ₆ N ₂ O ₅ PPd	C ₁₄ H ₁₄ AgCl ₂ F ₃ N ₂ O ₇ PdS	C ₁₂ H ₁₂ Ag ₂ N ₄ O ₁₀ Pd
Moiety formula	C ₁₂ H ₁₂ AgN ₂ O ₄ Pd, PF ₆ , CH ₃ OH	C ₁₂ H ₁₂ AgN ₂ O ₄ Pd, CF ₃ SO ₃ , CH ₂ Cl ₂	C ₁₂ H ₁₂ Ag ₂ N ₂ O ₄ Pd, 2 NO ₃
Formula weight (g/mol)	639.53	696.50	694.40
Crystal description	yellow plate	yellow prism	yellow rod
Crystal size (mm)	0.29 x 0.17 x 0.10	0.14 x 0.10 x 0.04	0.11 x 0.05 x 0.04
Crystal system	triclinic	triclinic	monoclinic
Space group	<i>P</i> $\bar{1}$	<i>P</i> $\bar{1}$	<i>P</i> 2 ₁ / <i>c</i>
<i>a</i> (Å)	9.358(4)	9.9183(13)	4.6283(8)
<i>b</i> (Å)	10.882(5)	10.7825(14)	25.815(4)
<i>c</i> (Å)	10.968(4)	11.6604(15)	7.8121
α (°)	116.299(6)	65.896(2)	
β (°)	96.468(6)	71.7491(19)	105.265(2)
γ (°)	91.599(6)	88.957(2)	
<i>V</i> (Å ³)	991.2(7)	1072.3(2)	900.5(3)
<i>Z</i>	2	2	2
μ (mm ⁻¹)	2.058	2.163	3.205
Total/unique reflections	7996/3479	15506/5733	10789/1878
<i>R</i> _{int}	0.0447	0.0443	0.0323
<i>R</i> [<i>F</i> ² > 2 σ (<i>F</i> ²)]	0.0592	0.0374	0.0180
w <i>R</i> ₂ (<i>F</i> ²)	0.1765	0.0838	0.0440
GOF	1.091	0.992	1.071
No. of parameters	268	287	135
$\Delta\rho_{\max}/\Delta\rho_{\min}$ (<i>e</i> Å ⁻³)	2.544 ^f /-1.648 ^g	0.912/-0.857	0.445/-0.556
CCDC	1005522	1005523	1005524

Table 5 Crystal data and refinement results of the bimetallic coordination polymers **5**, **6**, and **7**. f: highest peak 2.544 is 0.97 Å from Pd1; g: deepest hole -1.648 is 0.94 Å from Pd1.

$\text{Pd}(\text{acacCN})_2$ and $\text{Ag}(\text{I})$ salts aggregate to a 3D network or 1D chains. The latter topology provides an example for a tunable phase transition.



37x17mm (300 x 300 DPI)